CFD VALIDATION AGAINST LARGE SCALE LIQUEFIED HELIUM RELEASE

A.G. Venetsanos[1], S. Giannissi[1], C. Proust[2]
[1] Environmental Research Laboratory, National Centre for Scientific Research Demokritos,
15310 Aghia Paraskevi, Attikis, Greece, venets@ipta.demokritos.gr
[2] INERIS, Parc Technologique ALATA, BP2, Verneuil en Halatte 60550, France

Keywords: Liquefied Helium release, two-phase CFD, ADREA-HF

Abstract

The ADREA-HF CFD code is validated against a large scale liquefied helium release experiment on flat ground performed by INERIS in the past. The predicted release and dispersion behavior is evaluated against the experimental using temperature time histories at sensors deployed at various distances and heights downstream the source. For the selected sensors the temperature predictions are generally in good agreement with the experimental with a tendency to under-predict temperature as the source is approached.

1 INTRODUCTION

In a hydrogen based society liquefied hydrogen is an attractive option for hydrogen storage, due to its high storage density. Before though extensive use of liquefied hydrogen storage will become possible, potential safety issues regarding dispersion of liquefied hydrogen releases should be thoroughly examined and scrutinized, using experiments and simulations.

Earlier work on the subject consists of large scale liquefied hydrogen spill experiments performed by NASA [1] in 1984. These experiments were later simulated by [2], [3] and [4], using ADREA-HF, FLACS and FLUENT CFD codes, using different approaches regarding source modeling as well as phase change modeling.

In 1998, INERIS performed a series of 9 large scale experiments by releasing liquefied helium (for safety as a surrogate of hydrogen) on flat ground and monitoring temperature histories downstream at more than 100 sensors installed on a vertical rectangular frame 130 × 50 m in length and height [5, 6]. Modeling of these experiments does not exist in the literature.

In the present work we have selected Test-3 of the above INERIS tests, due to the experimentally observed good alignment of wind with sensors frame.

2 EXPERIMENTAL DESCRIPTION

In Test-3, a total estimated mass of 110 kg of helium was released in 52 s (mass flow rate of 2.1154 kg/s) from 3 bar absolute storage pressure. The release was equally distributed in two helium lines, each ending to a diffuser with hexagon exit section of 50 cm diameter and pointing downwards. The diffusers were horizontally close to each other, see Figure 1. Eight steel plates 1 × 2 m each were placed one besides the other on the ground below the diffusers, forming a 4 × 4 m steel pond, see Figure 1. Meteorological conditions consisted of: wind speed 2.5 m/s at 2.5 m height from ground, ambient temperature 12 C and 84% relative humidity.

During the experiment temperature histories were monitored downstream from the source location at more than 100 temperature sensors installed on a vertical rectangular frame 130 × 50 m in length and height.

Figure 1 Discharge layout showing discharge lines, diffusers and steel pond

3 MODELLING STRATEGY

Simulations were performed using the ADREA-HF code [7]. ADREA-HF code is a transient 3d multicomponent and multiphase pressure based CFD solver. Using the dispersed mixture approach, the code solves conservation equations for mixture mass, mixture momentum, mixture enthalpy and component total mass fractions. Homogeneous equilibrium is assumed between phases (same velocities, pressure and temperature). Liquid phase appearance exists when pressure is above the dew pressure of the mixture at given temperature (or equivalently when the temperature is below the dew temperature of the mixture at given pressure). Then phase distribution is obtained using Raoult's law for ideal mixtures, implemented using Rachford-Rice algorithm (PT-flasher). Given that the code solves for the mixture enthalpy, the mixture temperature and phase distribution for each substance are obtained for given mixture enthalpy, pressure and mass fractions using a Pressure-Enthalpy flasher algorithm (PH-flasher).

Simulations were performed in three stages. The first stage includes a one dimensional (in the Z direction) simulation to establish the ambient vertical profiles of velocity and turbulence. A constant velocity boundary condition was used at the top of the domain. The selected top velocity was such to produce the experimentally observed 2.5 m/s at 2.5 m height. A temperature lapse rate corresponding to neutral ambient atmospheric conditions was used, with 285.15 K at the domain bottom boundary. The second stage includes calculation of the 3d steady state flow, accounting for the effect of the diffuser as an obstacle. The third stage is the transient dispersion calculation. The working fluid was dry air and humidity (H_2O) in the first two stages, while helium was added in the third stage. A water mass fraction of 7.093e-3 was used to produce 84% relative humidity in the ambient air before the release starts. The water mass fraction varies during the dispersion calculation due to the presence of helium. Dry air is assumed to have a constant composition and remain always in the vapor state (infinitely large saturation pressure). Freezing of water was accounted when mixture temperature drops below water triple point temperature 273.2 K.

The ideal gas law was used to calculate vapor densities. Correlations from literature were used to calculate liquid densities of helium and water. Correlations from literature (in terms of temperature) were used to calculate all the other necessary physical properties for liquid and vapor per substance: specific heat under constant pressure, dynamic viscosity, conductivity, enthalpy of vaporization, enthalpy of freezing and liquid-vapor saturation pressure. Special attention should be drawn to the handling of helium vapor specific heat at temperatures close to saturation. Similar to hydrogen, helium vapor specific heat gradually increases at 1 bar as saturation temperature (4.23 K) is approached: 9082.7, 5250.8 and 5193.1 J/kg/K at 4.23, 20 and 30 K respectively. The higher vapor specific heat implies lower temperatures, lower densities and therefore more pronounced dense gas behavior. When comparing cryogenic hydrogen to cryogenic helium special attention should also be given to their pronounced difference regarding enthalpy of vaporization. At 1 bar, enthalpy of vaporization of

helium is approximately 23 times lower than that of hydrogen (with values 20.7 and 473.4 kJ/kg respectively). This implies that liquid helium will turn into vapor much faster than hydrogen.

The 3d computational domain extends from -10 to 150 m in X direction, from 0 to 20 m in Y direction and 0 to 40 m in the Z direction. Symmetry was assumed in the Y direction. In the present simulations the diffuser internal (and external) part is modeled. Diffuser surface was built in a step-wise approach with every diffuser surface part coinciding with a grid cell surface. The diffuser cross section (horizontal) area is 0.071 × 0.071 m at the top and 0.497 × 0.497 m at the bottom. The vertical distance between top and bottom of the diffuser is 0.426 m. The vertical distance between bottom of diffuser and ground is 0.142 m. The top area of the diffuser centered at coordinates (-2, 0.2485, 0.568) is used as the helium releasing source. The source area corresponds to a circular diameter of 8 cm. Modeled diffuser geometry, steel plate and horizontal grid near diffuser is shown in Figure 2.

The grid is Cartesian comprised of 88 × 39 × 96 = 329472 cells in the X, Y, Z directions. The minimum cell size is 0.071 m. This is used in the diffuser region (in all directions), close to ground and close to the symmetry plane. Far from these regions the grid is expanding with expansion factors not greater than 1.12. Maximum cell sizes in the X, Y and Z directions are 5.5, 2.1 and 2.5 m close to the East, North and top domain boundaries respectively. Two grid cells in the vertical direction were used between steel plate and diffuser to account for possibility of inflow of air to the region below the diffuser.

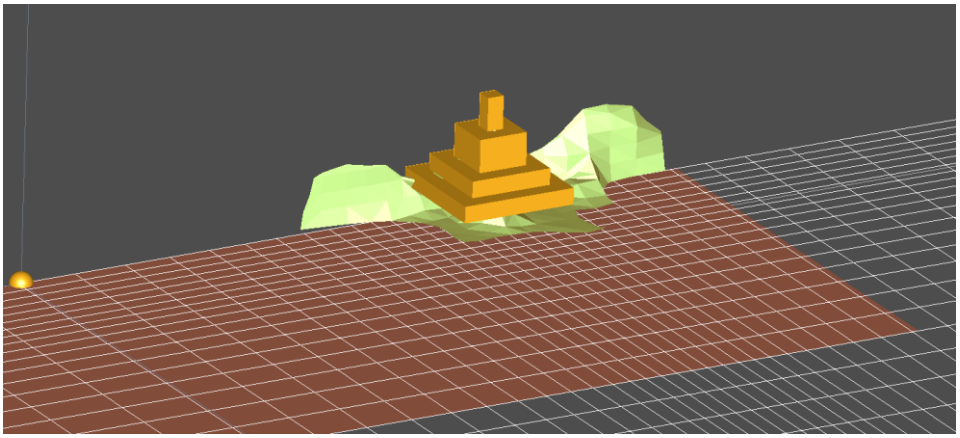

Figure 2 Modeled diffuser geometry, steel plate and horizontal grid near diffuser. Predicted 96% helium molar concentration cloud at time 1 sec

The simulations include solution of 1d energy equation in the underground (below the domain bottom boundary). Two underground layers were used in the region of the steel plate: 0.01 m steel on top and 0.06 m of sand below. One underground layer (0.06 m of sand) was used for the rest of the bottom domain. Sand was assumed to have 5% moisture content. Underground grid is equidistant with size 0.0025 m resulting in 4 cells within steel and 24 cells within sand. A constant temperature of 285.15 K was used as boundary condition at the bottom of the sand layer. Heat flux consistency was used as boundary condition between underground and ambient, i.e. heat flux from the ambient side should equal heat flux from the underground side. An initial temperature of 285.15 was used throughout the underground.

Standard wall functions were used for velocity temperature and turbulence to bridge the area between solid boundaries and center of adjacent computational cells. Hydrodynamic roughness values were set to 0.0001 m for steel and 0.008 m for sand.

Turbulence was modeled using the standard k-ε model, with account of stability. Turbulent Prandtl and Schmidt numbers were set both to 0.72.

The MUSCL scheme (second order) was used for convective discretization of all solved variables and density. Besides its increased accuracy, use of the MUSCL scheme is particularly important in order to

avoid butterfly effects when impinging jet flow is present in the solution domain, as occurs in the present simulations. The fully implicit backwards Euler scheme (first order) was used for time discretization, with a maximum permitted Courant-Friedrichs limit = 2 for time step control. This condition resulted in a time step of approximately 0.01 s and 0.04 s during and after the end of the release respectively.

Inlet boundary conditions were applied at the domain West plane and at the source. A constant pressure boundary condition was used for the normal velocities at the East, North and Top domain boundaries. Zero gradient if outflow or initial value if inflow, was used as boundary condition for the remaining variables at these boundaries. Symmetry boundary condition was applied at the domain South plane.

At the source saturated helium conditions were assumed: 1 atm pressure and 4.23 K. Uncertainty exists in the estimation of the source void fraction. At stagnation conditions (in storage tank) helium was sub-cooled at pressure 3 bara, which is higher than the critical pressure of helium (2.275 bar) and therefore its temperature was below the critical (5.195 K). The pressurization of the storage tank just before the release was very fast. By assuming an isentropic pressurization process from 1 atm to 3 bara, one gets a stagnation temperature of 4.465 K. By performing an isenthalpic expansion from stagnation conditions to ambient pressure one gets a source vapor quality of 0.075. Given the uncertainties in the source vapor quality estimation above and the increased propensity of helium to vaporize due to its very low vaporization enthalpy, in this work we performed simulations with vapor qualities of 0.5 and 1.0. Table below summarizes the release conditions used.

Table 1: Release conditions used in the simulations

Case	Temperature	Vapour quality	Void fraction	Density	Velocity
1	4.2	0.5	0.914	21.235	9.88
2	4.2	1.0	1.0	11.613	18.07

4 RESULTS AND DISCUSSION

Figure 2 shows predicted 96% helium molar concentration cloud at time 1 sec after start of release, for source vapor fraction 1.0. Helium jet, emitted internally from diffuser top is shown to hit the ground and spread horizontally.

Predicted visible cloud on the symmetry plane at time 50 s is shown in Figure 3. Cloud visibility is enabled when water liquid is present in the atmosphere and this happens when the temperature is below the dew temperature of the mixture. Visible cloud just before the end of the release has reached a horizontal distance of approximately 87 m downstream from the source and a maximum vertical elevation of approximately 20 m.

Predicted distribution of helium molar concentration on the symmetry plane at time 50 s is shown in Figure 4. Equivalent hydrogen flammable cloud (i.e. 4% concentration) has reached a horizontal distance of approximately 37 m downstream from the source and a maximum vertical elevation of approximately 14 m.

Predicted temperature distribution on the symmetry plane at time 50 s is shown in Figure 5. A temperature drop of 2 K is observed to have reached a horizontal distance of approximately 140 m downstream from the source.

A comparison between predicted and experimental temperature time series is shown in Figure 6. The selected temperature sensor locations are shown by circles in Figure 5. Predicted results are shown for both adopted modeling options regarding helium vapor fraction at the source.

At the sensor T101 located closest to the source predicted temperatures are close to 50 K, while experimental temperatures are generally higher but with a minimum of approximately 50 K. A small difference is observed between the two modeling options.

At sensor T101 large oscillations are observed in the experimental temperature time series, the origin of which is not very clear. Such oscillations do not exist in the predictions at the same location. Further away from the source, experimental temperature oscillations decrease with distance from source, leading to the suggestion that the large oscillations near the source must be due to the release itself.

A large decrease in temperature compared to ambient is observed computationally and experimentally at sensors T302 and T503. A large difference is observed between the two modeling options at these locations. Prediction with source vapor fraction 1.0 gives lower temperatures than with vapor fraction 0.5, meaning that in the second case the cloud has been more attached to the ground and therefore affected the given elevated sensors less. Compared to the experimental data, the prediction with 0.5 source vapor fraction gives more consistent results.

For the remaining sensors at larger distances from the source, predictions are generally in relatively good agreement with the experiments and the effect of the source vapor fraction on the predicted temperatures is rather small.

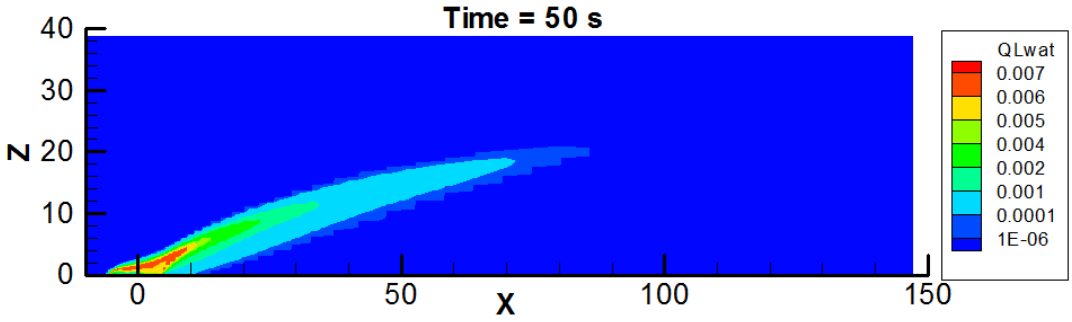

Figure 3 Predictions on the symmetry plane of water liquid fraction. Calculation with source vapor quality x = 1.0.

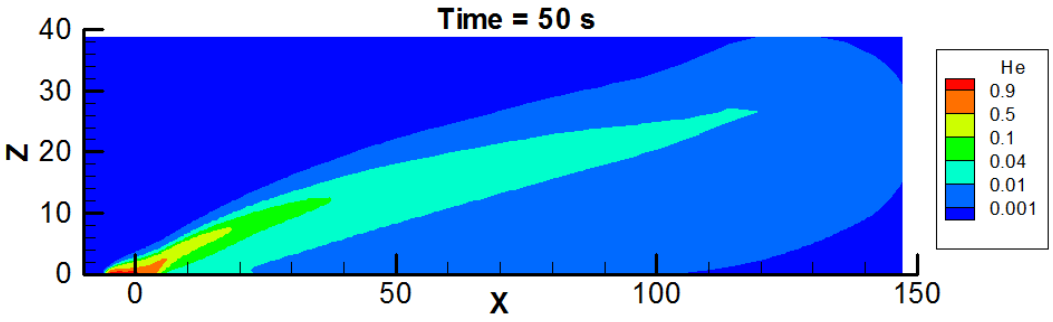

Figure 4 Predictions on the symmetry plane of helium molar concentration. Calculation with source vapor quality x = 1.0.

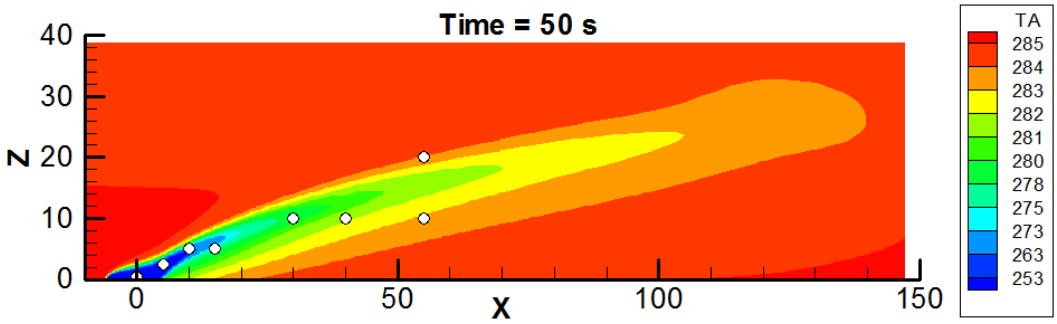

Figure 5 Predictions on the symmetry plane of temperature distribution. Calculation with source vapor quality x = 1.0. Circles represent selected sensor locations.

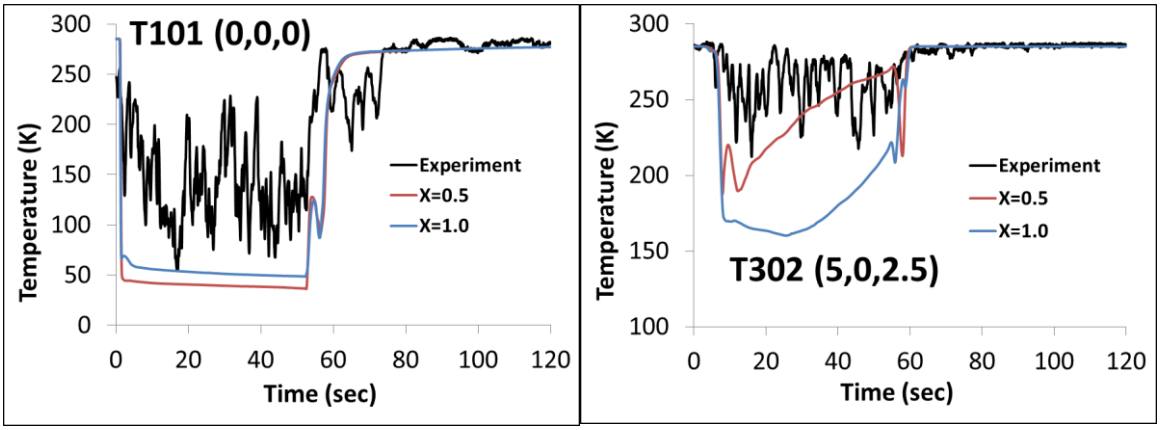

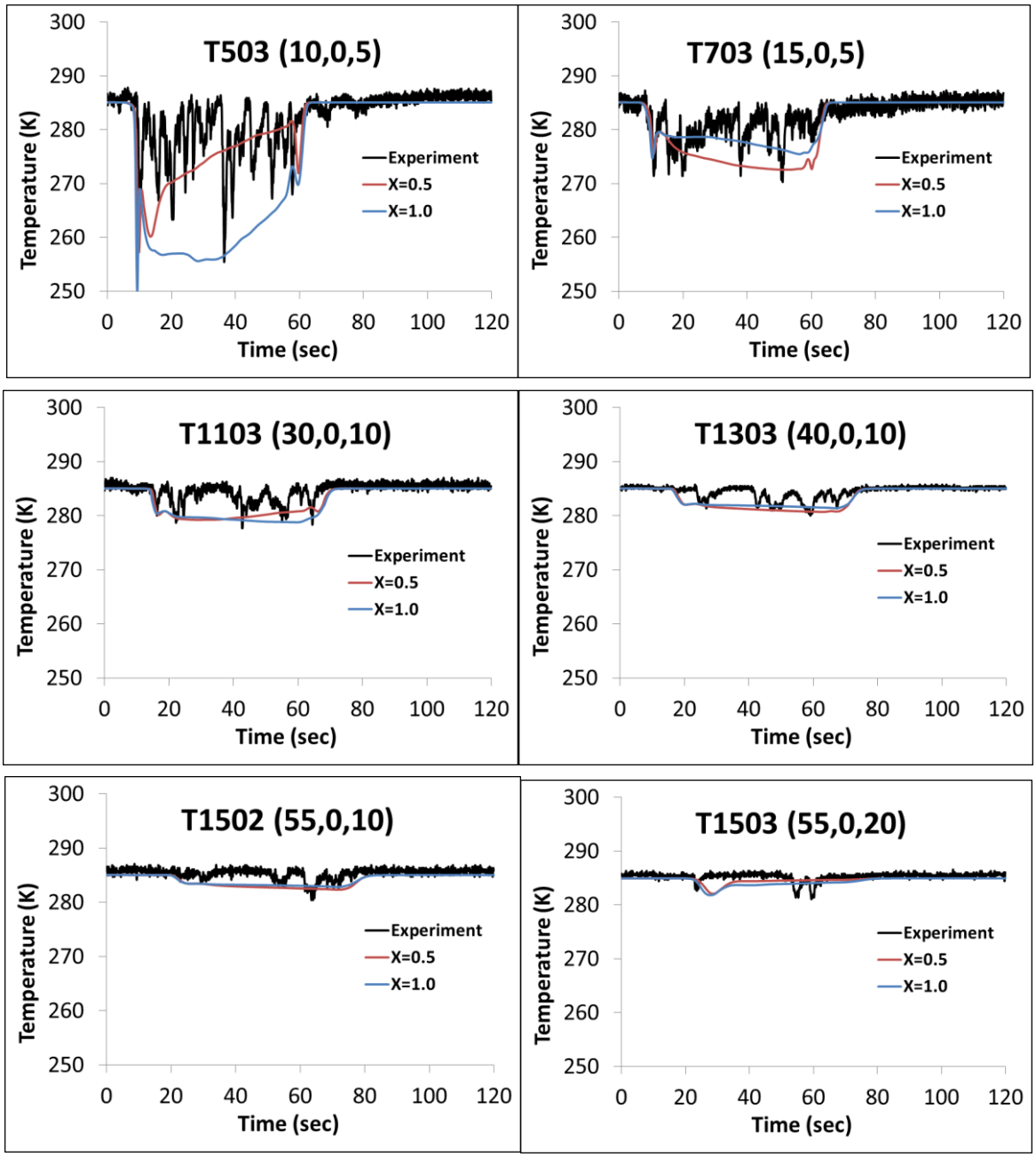

Figure 6 Comparison between predicted and experimental temperature times series at selected sensor locations. Title shows name of experimental sensor and its X, Y, Z coordinates

5 CONCLUSIONS

In this work we have validated the ADREA-HF CFD code against INERIS Test-3 experiment involving a large scale release of 110 kg of helium in 52 s on flat ground.

The predicted dispersion behavior has been qualitatively evaluated against the experimental using temperature time histories at sensors deployed at various distances and heights downstream the source. For the selected sensors the temperature predictions are generally in good agreement with the experimental with a tendency to under-predict temperature as the source is approached.

6 ACKNOWLEDGEMENTS

The research leading to these results was financially supported by the PRESLHY project, which has received funding from the Fuel Cells and Hydrogen 2 Joint Undertaking under the European Union's Horizon 2020 research and innovation program under grant agreement No 779613.

7 REFERENCES

1 Witcofski R.D., Chirivella J.E., Experimental and analytical analyses of the mechanisms governing the dispersion of flammable clouds formed by liquid hydrogen spills, Int. J Hydrogen Energy 9 (1984) 425–435.

2 Venetsanos A.G., Bartzis J.G., CFD modelling of large-scale LH2 spills in open environment, Int. J. Hydrogen Energy, 32 (2007), 2171-2177.

3 Middha P., Ichard M., Arntzen B.J., Validation of CFD modelling of LH2 spread and evaporation against large-scale spill experiments, Int. J. Hydrogen Energy 36 (2011) 2620–2627

4 Liu Y., Wei J., Lei G., Lan Y., Chen H., Jin T., Dilution of hazardous vapor cloud in liquid hydrogen spill process under different source conditions. Int. J. Hydrogen Energy 43 (2018) 7643–7651

5 Proust C., Chelhaoui S., Joly C., Processes of the formation and explosion of hydrogen-air clouds following an extensive spillage of liquid hydrogen, National Hydrogen Association 12th Annual U.S. Hydrogen Meeting and Exposition, 2001

6 Proust C., Lacome, J.M., Jamois, D., Perrette, L., Processes of the formation of large unconfined clouds following a massive spillage of liquid hydrogen on the ground, 2nd International Conference of Hydrogen Safety, San Sebastian, Spain, 2007

7 Venetsanos A.G., Papanikolaou E., Bartzis J.G., The ADREA-HF CFD code for consequence assessment of hydrogen applications, Int. J. Hydrogen Energy 35 (2010) 3908–3918